

Supporting Information for

Sc³⁺-promoted O–O bond cleavage of a (μ -1,2-peroxo)diiron(III) species formed from an iron(II) precursor and O₂ to generate a complex with an Fe^{IV}₂(μ -O)₂ core

Saikat Banerjee,^[a] Apparao Draksharapu,^[a] Patrick M. Crossland,^[a] Ruixi Fan,^[b] Yisong Guo,^{*,[b]} Marcel Swart,^{*,[c,d]} and Lawrence Que, Jr.^{*,[a]}

^[a] Department of Chemistry and Center for Metals in Biocatalysis, University of Minnesota, Minneapolis, Minnesota 55455, United States

^[b] Department of Chemistry, Carnegie Mellon University, Pittsburgh, PA 15213, USA

^[c] ICREA, Pg. Lluís Companys 23, 08010 Barcelona, Spain

^[d] IQCC & Dept. Chem., University of Girona, 17003 Girona, Spain

Table of Contents

1. Mössbauer spectroscopy	S2
2. X-ray Absorption spectroscopy	S7
3. Resonance Raman spectroscopy	S13
4. UV-vis studies and related kinetic analyses	S14
5. DFT Calculations and Results	S18
6. References	S26

1. Mössbauer spectroscopy

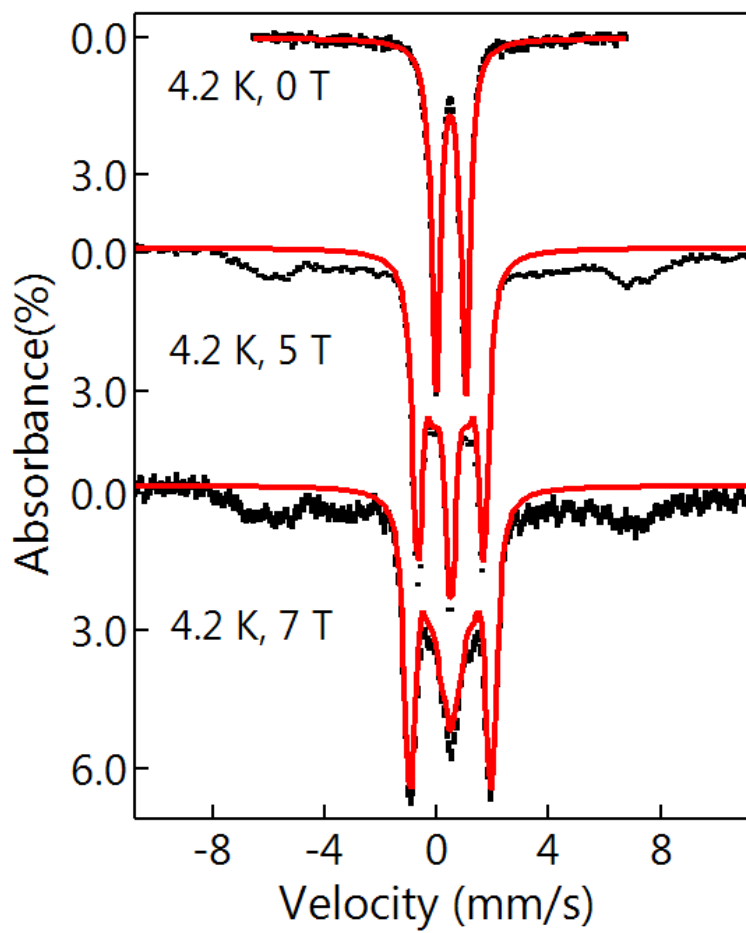


Figure S1: Mössbauer spectra of **2** measured at 4.2 K with various applied fields (0 T, 5 T, 7 T). The red solid lines represent the spectral simulation of an $S = 0$ peroxodiiron(III) species, representing ~80% iron in the sample. The black arrows indicated possible high-spin ferric impurities.

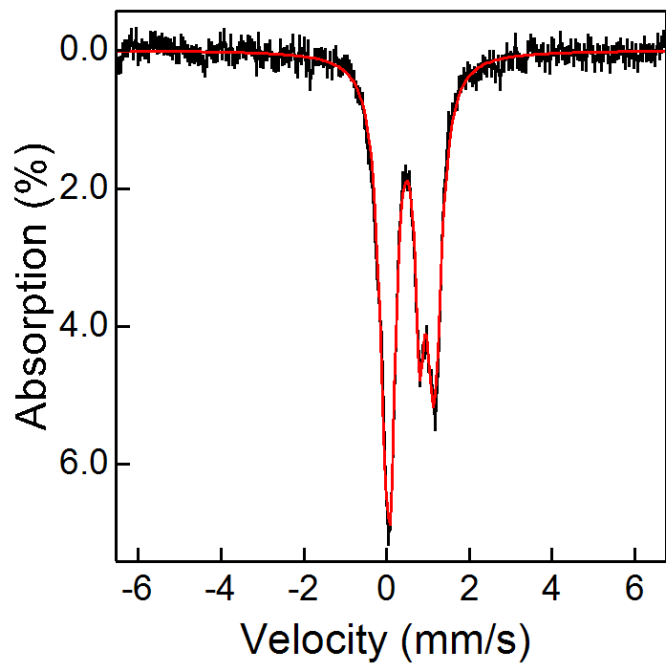


Figure S2: Mössbauer spectra of **2+H⁺** measured at 4.2 K and 0 T.

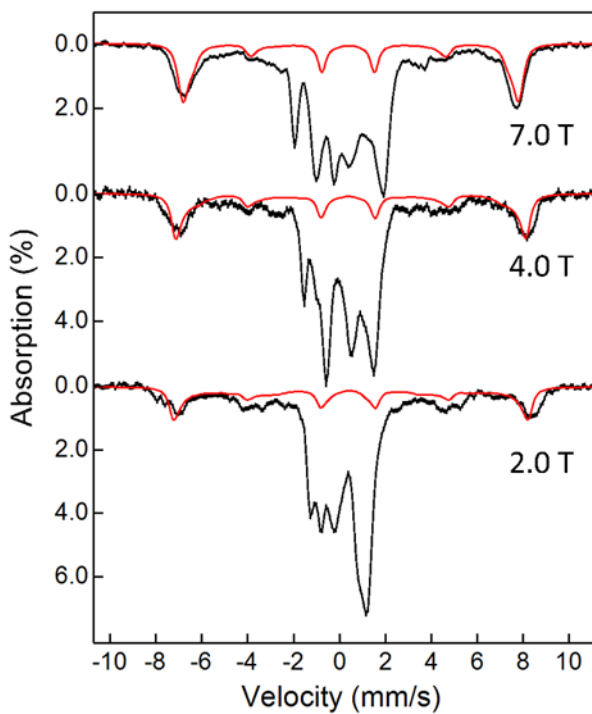


Figure S3. 4.2 K Mössbauer spectra of **3** (with various applied magnetic fields, 2.0T, 4.0T, 7.0T respectively). Black: experimental spectra; red: the theoretical simulation of a typical high-spin ferric species, representing mono-ferric impurities in the sample that occupies

~20% of the total iron. Please note that this mono-ferric simulation is only for the purpose of estimating the contribution of this species in the spectra in order to remove it for further analysis of the majority iron species in the sample (see Figure S4).

Table S1: Simulation parameters used in fitting the spectral components of **3** shown in Figure S4.

Species	Diiron(IV) component	Diiron(III) component
Spin state	$S = 0$	$S = 0$
Isomer shift (mm/s)	-0.04	0.48
Quadrupole splitting (mm/s)	2.00	-1.22
η	0.4	0.9
Line width (mm/s)	0.3	0.50
Percentage (%)	35 %	35%

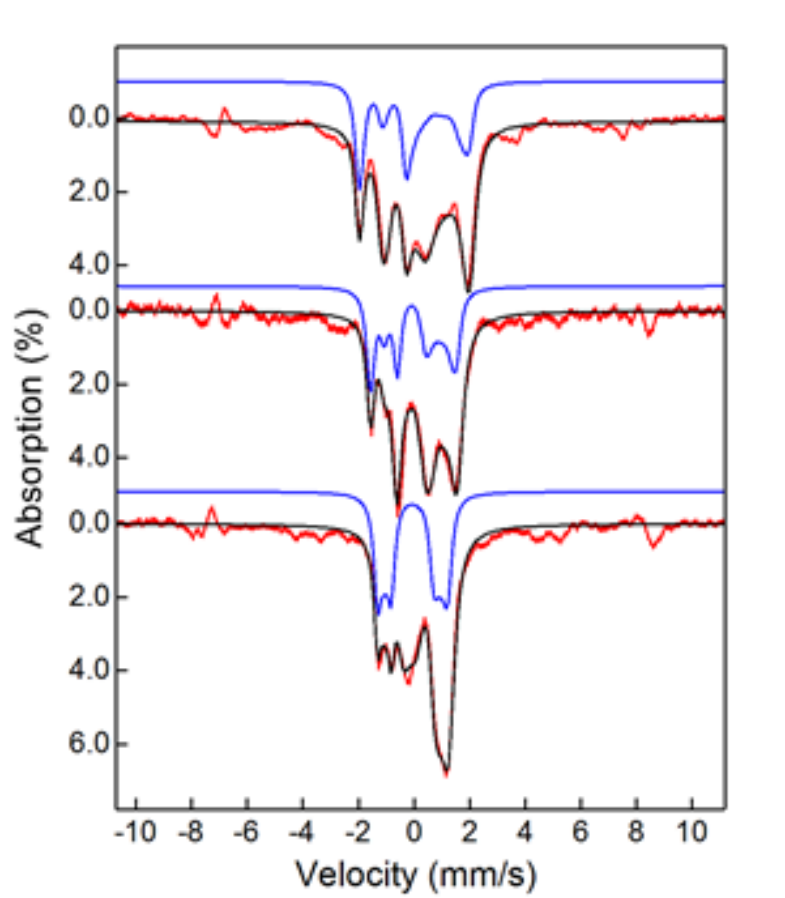


Figure S4: 4.2 K Mössbauer spectra of **3** (with various applied magnetic fields (2.0T, 4.0T, 7.0T respectively)). Red: experimental spectra of the sample after removal of high-spin ferric impurities (See Figure S3); black: the theoretical simulations of the sum of the diiron(III) and diiron(IV) components; blue: the theoretical simulations of only the diiron(IV) component. See Table S1 for simulation parameters.

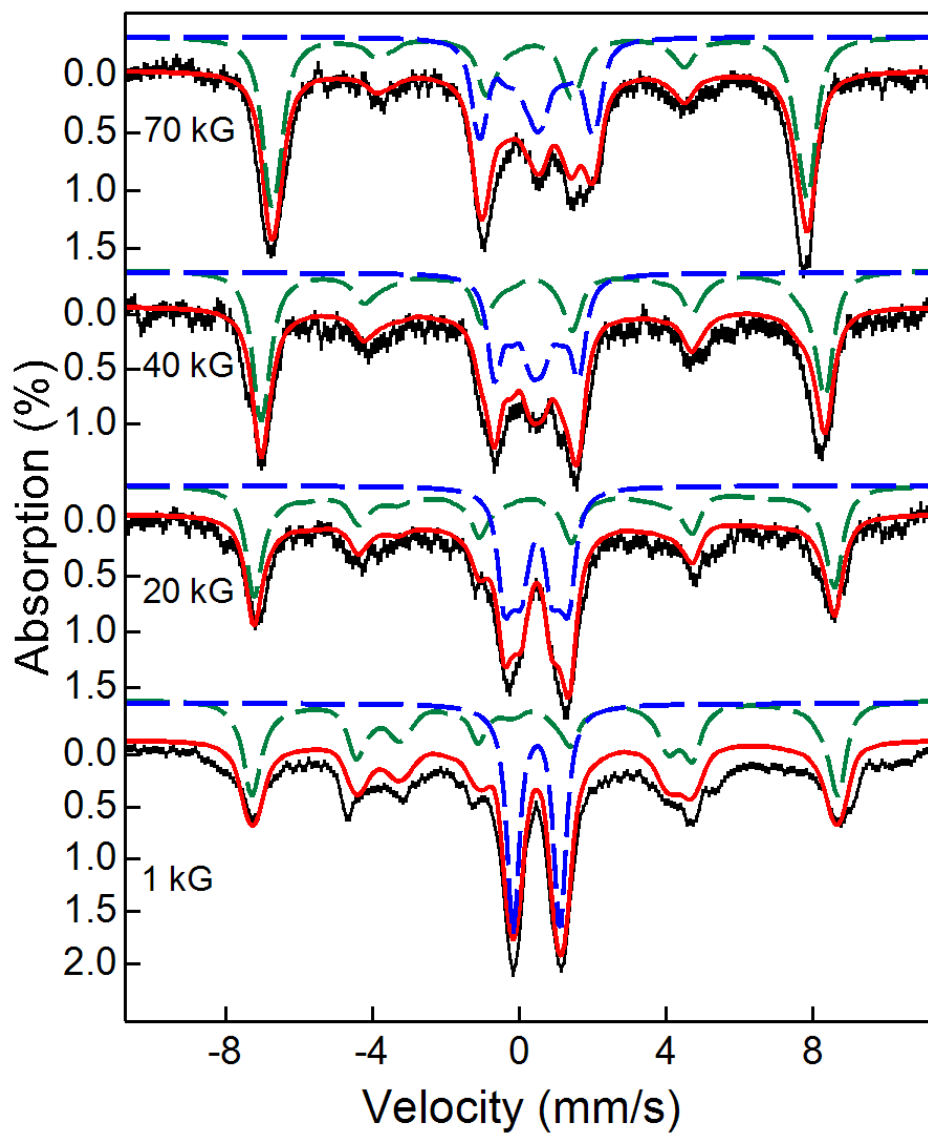


Figure S5: 4.2 K Mössbauer spectra of decayed product of **3** measured under various applied magnetic fields (7 T, 4 T, 2 T, 0.1 T). Black: experimental spectra; red: the theoretical simulations of the sum of the diiron(III) and high-spin mono-ferric species; blue: the theoretical simulations of the diiron(III) species with parameters of $\delta = 0.48$ mm/s and $\Delta E_Q = -1.22$ mm/s, representing ~40% of the total iron in the sample; green: the theoretical simulation of a high-spin mono-ferric species with parameters of $D \sim 1$ cm⁻¹, $E/D = 0.33$, $\delta = 0.43$ mm/s, $\Delta E_Q = -0.58$ mm/s, $\eta = 1.5$, $A_x = A_y = A_z \sim -21$ T, representing ~60% of the total iron. Please note that the parameters used for simulating the mono-ferric species are only for the purpose of estimating the relative concentration of this species. More analyses need to be carried out to exclusively determine all the parameters, which is beyond the scope of the current study.

2. X-ray Absorption Spectroscopy

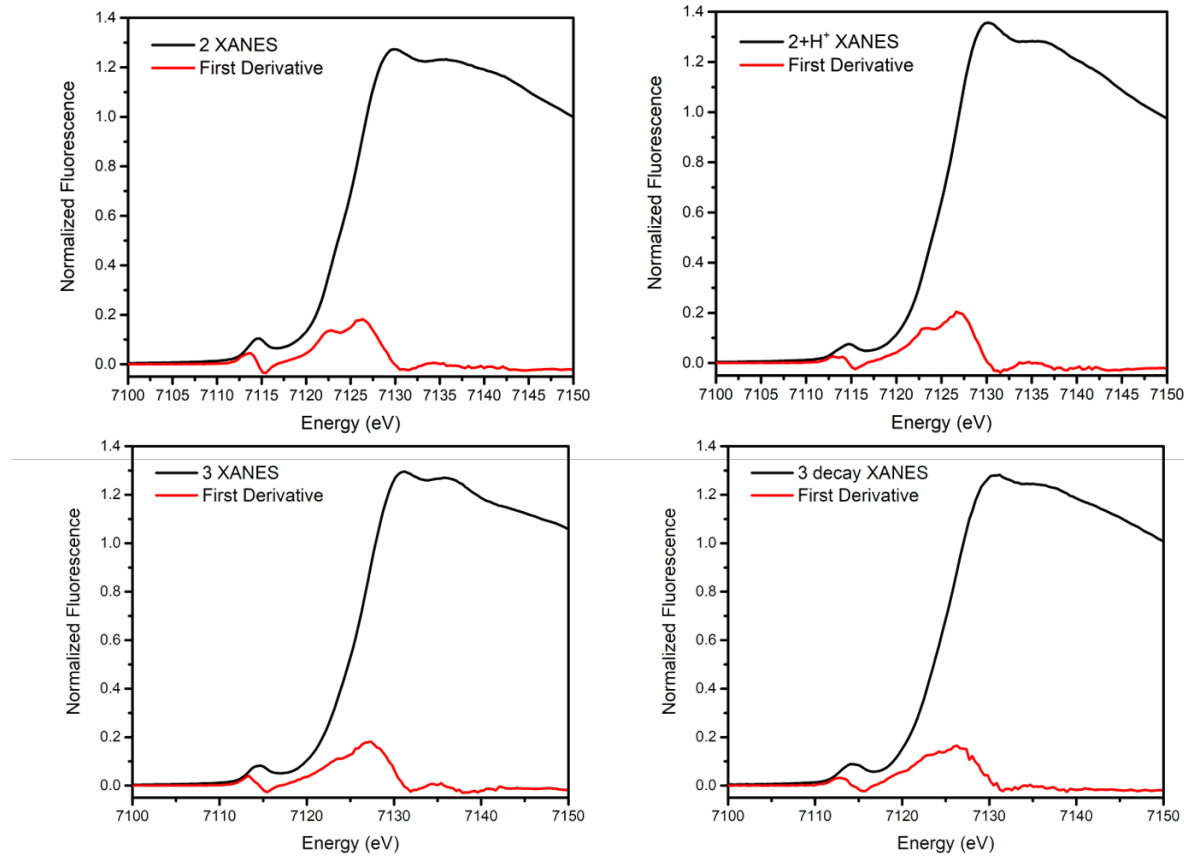


Figure S6a. Fe K-edge XANES features for **2** (top left), **2+H⁺** (top right), **3** (bottom left), and decayed **3** (bottom right).

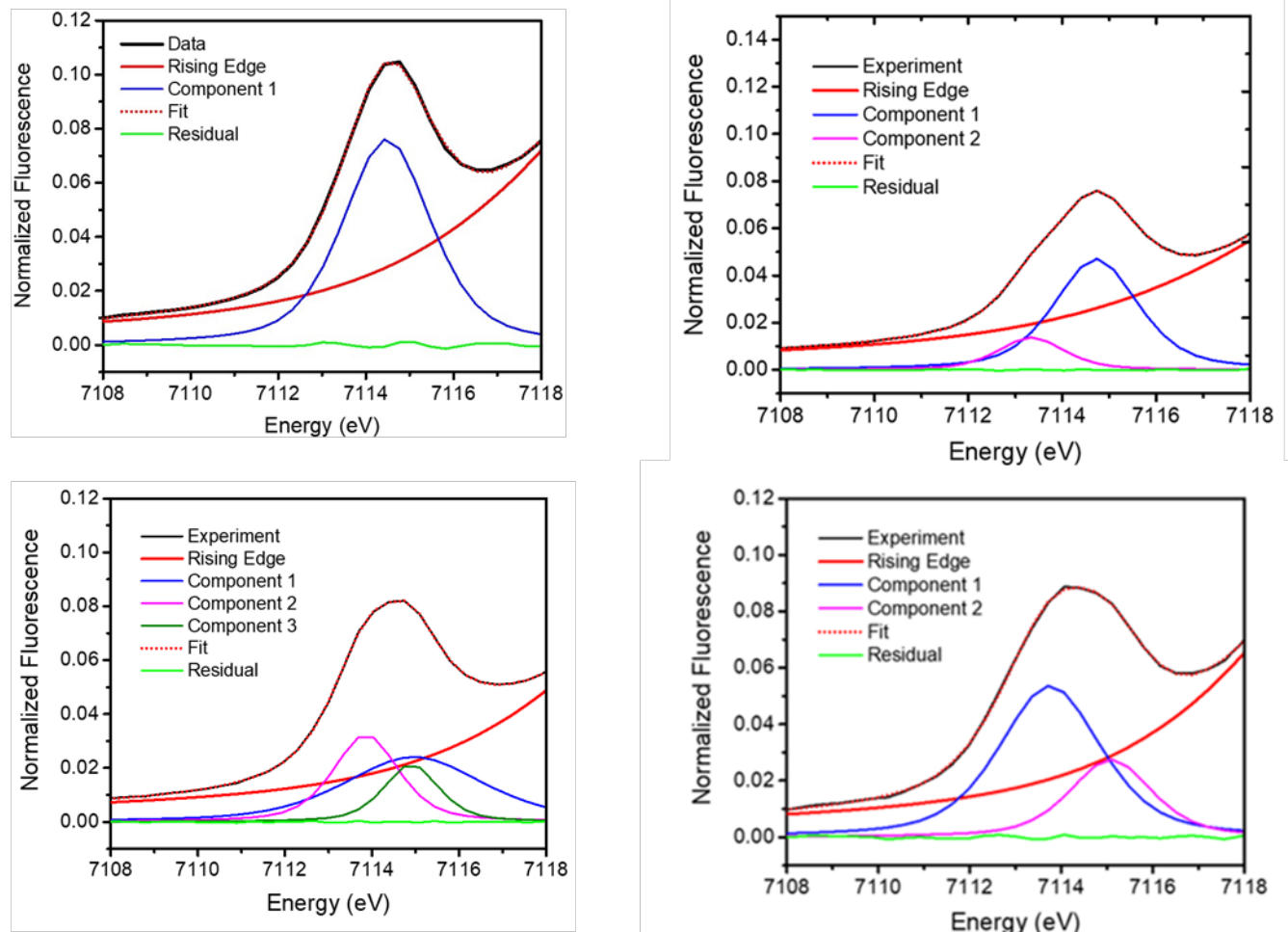


Figure S6b. Fe K-edge pre-edge features for **2** (top left), **2+H⁺** (top right), **3** (bottom left), and decayed **3** (bottom right).

Table S2. K-edge energies and pre-edge fitting parameters

Species	K-edge (eV)	Peak Position (eV)	Area (units)
2	7126.3	7114.5	18.2
2 + H⁺	7126.7	7114.7	9.9
		7113.3	2.3
		Total = 12.2	
3	7127.5	7115.0	9.2
		7113.9	5.8
		7114.9	3.2
		Total = 18.2	
Decayed 3	7126.3	7113.8	14.1
		7115.1	5.8
		Total = 19.9	

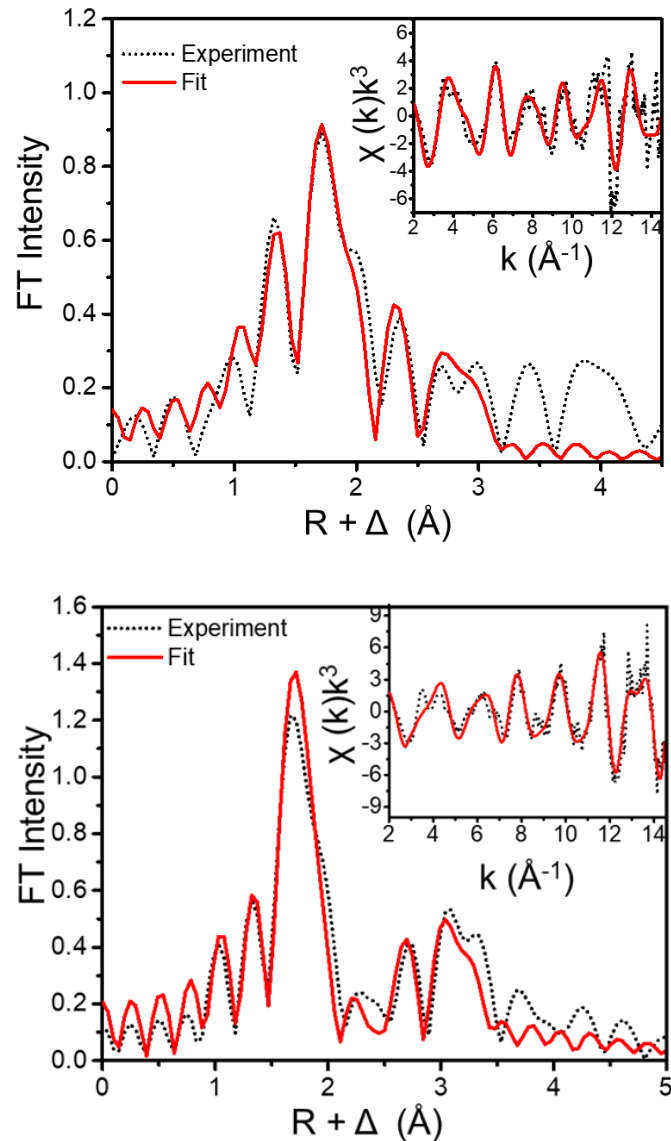


Figure S7. Fourier transformed and k-space (inset) EXAFS data (dotted black line) and best fit (red line) for **2 + H^+** (Top) and **3 decay** (Bottom).

Table S3. EXAFS fitting parameters for **2**, **3**, **2+H⁺** and decayed **3**; best fits in bold font

2				Fe-N/O				Fe-O/N				Fe...C/N				Fe...Fe				GOF		
Fit	N	R(Å)	$\sigma^2(10^{-3})$	N	R(Å)	$\sigma^2(10^{-3})$	N	R(Å)	$\sigma^2(10^{-3})$	N	R(Å)	$\sigma^2(10^{-3})$	E ₀	F	F'							
1	4	2.13	7.31	-	-	-	-	-	-	-	-	-	-	1.72	955	658						
2	4	2.12	4.55	2	1.85	5.03	-	-	-	-	-	-	-	-4.01	601	655						
3	4	2.12	4.61	2	1.85	5.14	-	-	-	1	3.06	6.95	-3.41	539	653							
4	4	2.11	4.85	2	1.84	4.90	3	2.91	3.57	1	3.06	3.57	-5.37	508	649							
5	4	2.11	5.08	2	1.84	4.92	3	2.94	-0.70	1	3.07	0.20	-3.24	466	646							
							3	3.24	0.68													
6	4	2.11	5.03	2	1.84	4.94	4	2.94	1.37	1	3.07	0.31	-3.56	468	646							
							3	3.24	0.56													
3				Fe-N/O				Fe-O/N				Fe...C/N				Fe...Fe				GOF		
Fit	N	R(Å)	$\sigma^2(10^{-3})$	N	R(Å)	$\sigma^2(10^{-3})$	N	R(Å)	$\sigma^2(10^{-3})$	N	R(Å)	$\sigma^2(10^{-3})$	E ₀	F	F'							
1	2	2.09	2.67	-	-	-	-	-	-	-	-	-	-	67.9	883	631						
2	2	2.04	2.34	2	1.81	6.83	-	-	-	-	-	-	-	-7.39	764	628						
3	2	2.01	-0.60	2	1.82	3.61	-	-	-	-	-	-	-	-2.41	696	626						
	2	2.13	0.09	-	-	-	-	-	-	-	-	-	-	-	-	-	-					
4	2	1.99	0.54	2	1.81	3.96	-	-	-	0.4	2.70	0.26	-3.95	535	623							
	2	2.11	0.57	-	-	-	-	-	-	-	-	-	-	-	-	-	-					
5	2	1.99	0.17	2	1.81	3.61	-	-	-	0.4	2.71	0.00	-4.08	522	621							
	2	2.11	0.01	-	-	-	-	-	-	0.4	2.90	8.66	-	-	-	-	-					
6	2	1.99	0.17	2	1.81	3.58	-	-	-	0.4	2.70	0.13	-3.97	527	621							
	2	2.11	0.09	-	-	-	-	-	-	0.4	3.28	6.31	-	-	-	-	-					
7	2	1.99	0.32	2	1.81	3.75	2	2.90	8.77	0.4	2.70	0.00	-3.02	505	618							
	2	2.11	0.20	-	-	-	-	-	-	0.4	3.28	7.05	-	-	-	-	-					
8	2	1.99	0.40	2	1.81	3.92	2	2.99	5.60	0.4	2.70	-0.20	-1.70	498	616							
	2	2.12	0.38	-	-	-	2	2.82	3.50	0.4	3.27	3.27	-	-	-	-	-					
9	2	1.99	0.28	2	1.81	3.72	2	2.91	8.40	0.4	2.71	0.01	-3.23	486	616							
	2	2.11	0.13	-	-	-	2	3.61	3.11	0.4	3.32	3.32	-	-	-	-	-					
10	2	1.97	0.22	2	1.79	4.15	2	2.90	6.40	0.4	2.70	0.07	-5.17	517	618							
	2	2.09	0.19	-	-	-	-	-	-	0.4	3.28	6.97	-	-	-	-	-					
11	2.4	1.95	3.46	1.2	1.78	1.15	2	2.92	7.48	0.4	2.71	0.00	-2.56	503	618							
	2.4	2.09	1.82	-	-	-	-	-	-	0.4	3.29	7.36	-	-	-	-	-					

2+H ⁺				Fe-N/O			Fe-O/N			Fe...C/N			Fe...Fe			GOF		
Fit	N	R(Å)	$\sigma^2(10^{-3})$	N	R(Å)	$\sigma^2(10^{-3})$	N	R(Å)	$\sigma^2(10^{-3})$	N	R(Å)	$\sigma^2(10^{-3})$	E ₀	F	F'			
1	4	2.10	3.49	-	-	-	-	-	-	-	-	-	1.91	732	470			
2	4	2.09	2.22	2	1.89	5.01	-	-	-	-	-	-	-5.22	648	469			
3	4	2.09	2.18	2	1.89	5.25	-	-	-	1	3.07	8.05	-4.69	629	467			
4	4	2.08	1.97	2	1.89	4.58	3	2.91	0.29	1	3.06	3.01	-4.89	590	465			
5	4	2.09	1.85	2	1.89	4.94	6	2.95	13.14	1	3.11	6.01	-4.02	587	455			
6	4	2.09	1.79	2	1.89	4.62	4	2.93	2.32	0.8	3.09	1.57	-4.55	585	457			
7	4	2.09	1.89	2	1.89	4.87	5	2.93	4.09	1	3.09	2.80	-4.37	594	457			
8	4	2.09	1.84	2	1.89	4.76	5	2.94	4.63	0.8	3.09	1.83	-4.27	591	456			

Decayed 3				Fe-N/O			Fe-O/N			Fe...C/N			Fe...Fe			GOF		
Fit	N	R(Å)	$\sigma^2(10^{-3})$	E ₀	F	F'												
1	6	2.07	3.94										-2.45	893	392			
2	4	2.07	1.13										-1.70	745	392			
3	4	2.05	2.11	1	1.82	-0.80							-4.01	569	391			
4	4	2.05	1.84	1	1.82	-1.00							-5.81	558	389			
				1	1.71	13.82												
5	4	2.05	0.94	2	1.83	2.86							-7.61	575	391			
6	4	2.06	1.00	2	1.83	3.49				1	3.36	1.44	-4.29	548	389			
7	4	2.07	0.92	2	1.83	3.03	4	2.91	2.81	1	3.36	1.89	-3.93	534	387			
8	4	2.07	0.95	2	1.83	4.07	4	2.96	3.46	1	3.34	1.01	-1.80	451	386			
							5	3.17	0.05									

3. Resonance Raman spectroscopy

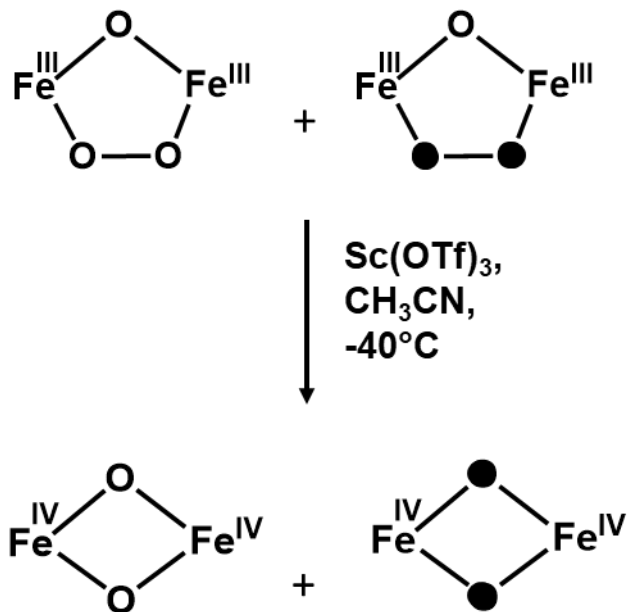
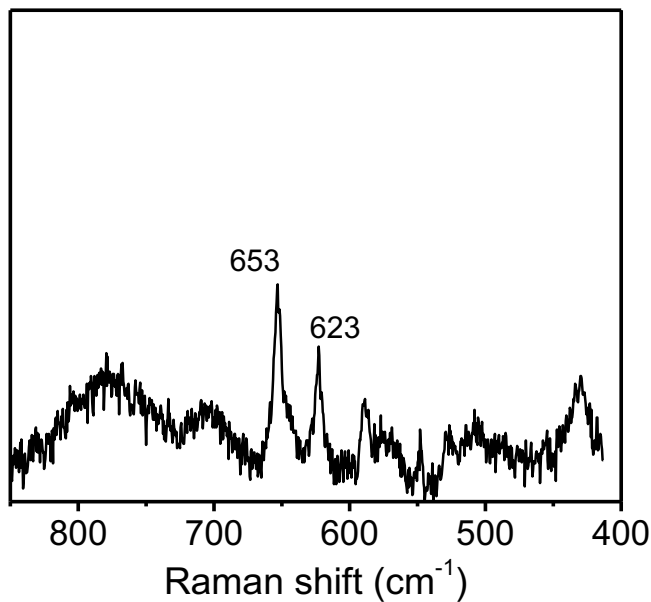


Figure S8: (Top) Resonance Raman spectra of **3** generated by adding $\text{Sc}(\text{OTf})_3$ to a mixture of $^{16}\text{O}_2\text{-2}$ and $^{18}\text{O}_2\text{-2}$ in CH_3CN at -40°C , demonstrating that mixed-labeled **3** does not form. (Bottom) Scheme showing the experimental results of the mixed labeling experiment. Filled oxygen atoms denote ^{18}O isotope and hollow oxygen atoms denote ^{16}O isotope.

4. UV-vis studies and related kinetic analyses

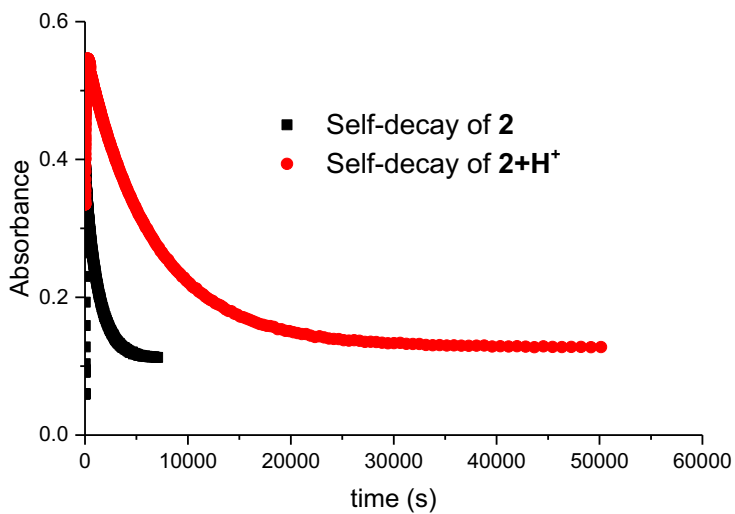


Figure S9: Comparison of self-decay curves of **2** and **2+H⁺** in CH₃CN at -40 °C.

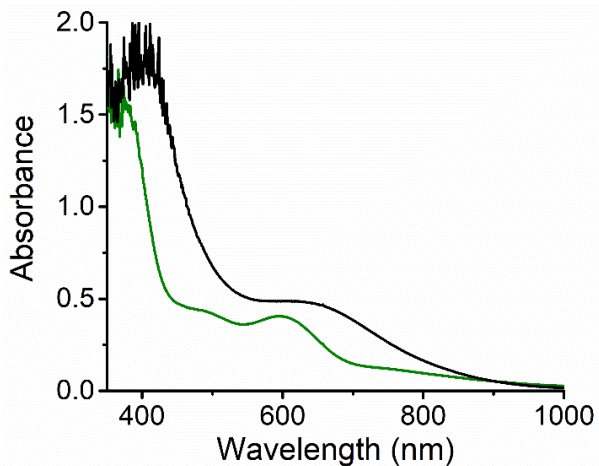


Figure S10: UV-vis spectra of the changes to **2** upon the addition of HClO₄ (1.5 equiv.) in CH₃CN at -40 °C. **2** was generated by adding (1.5 eq) DBU/H₂O to a 1 mM solution of **1** in CH₃CN.

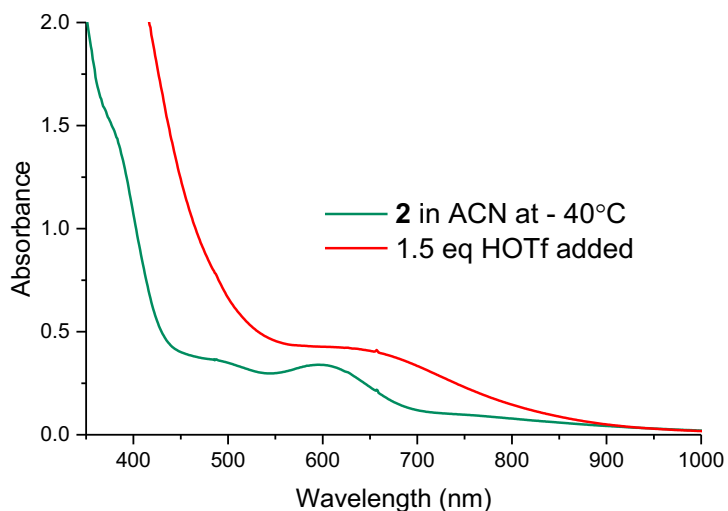


Figure S11: UV-vis spectra of the formation of **2+H⁺** (red) after the addition of triflic acid (1.5 eq) to a CH₃CN solution of **2** (green) at -40°C. **2** was generated by adding (1.5 eq) DBU/H₂O to a 1 mM solution of **1** in CH₃CN.

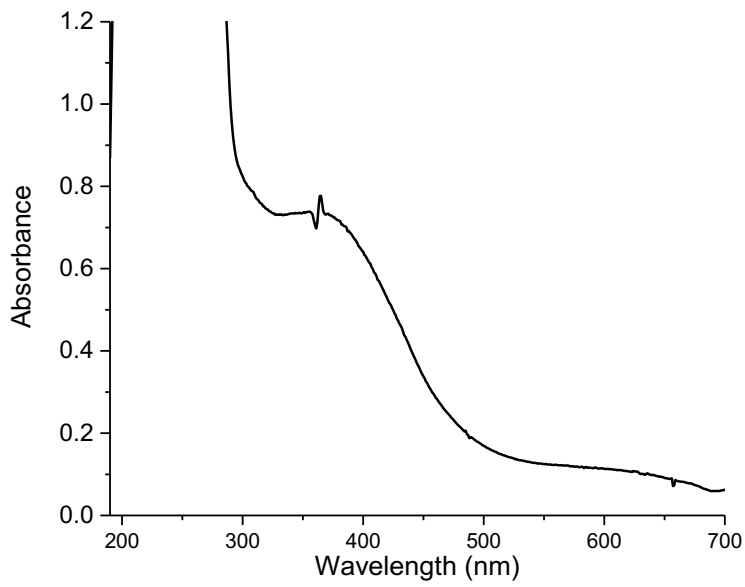


Figure S12: Near-UV-visible spectrum of **3** in CH₃CN at -40 °C. **3** was generated from **2** by the addition of (2 eq) Sc(OTf)₃ in a 0.5 cm cuvette. **2** was generated by adding (1.5 eq) DBU/H₂O to a solution of **1** (0.25 mM).

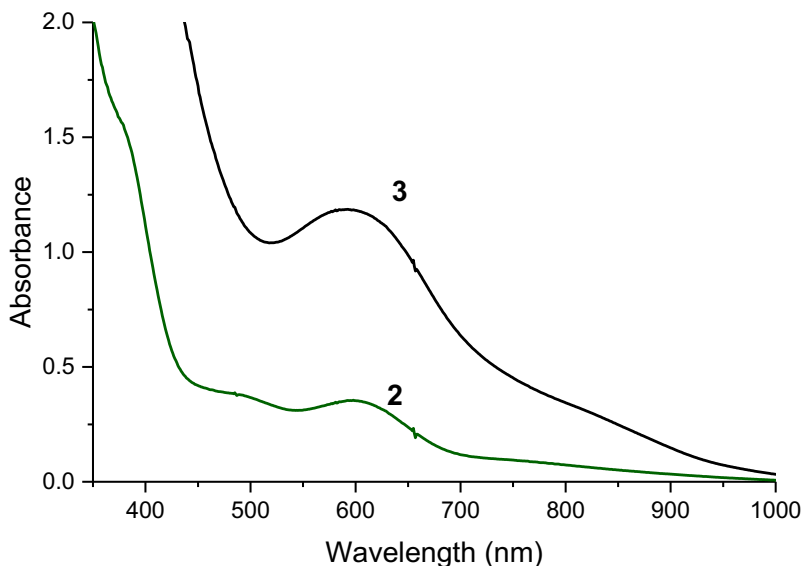


Figure S13: UV-vis spectra showing the formation of **3** (black) upon addition of $\text{Al}(\text{OTf})_3$ (2 eq) to a solution of **2** (green) in which solvent at -40°C . **2** was generated by adding (1.5 eq) DBU/ H_2O to a 1 mM solution of **1** in CH_3CN .

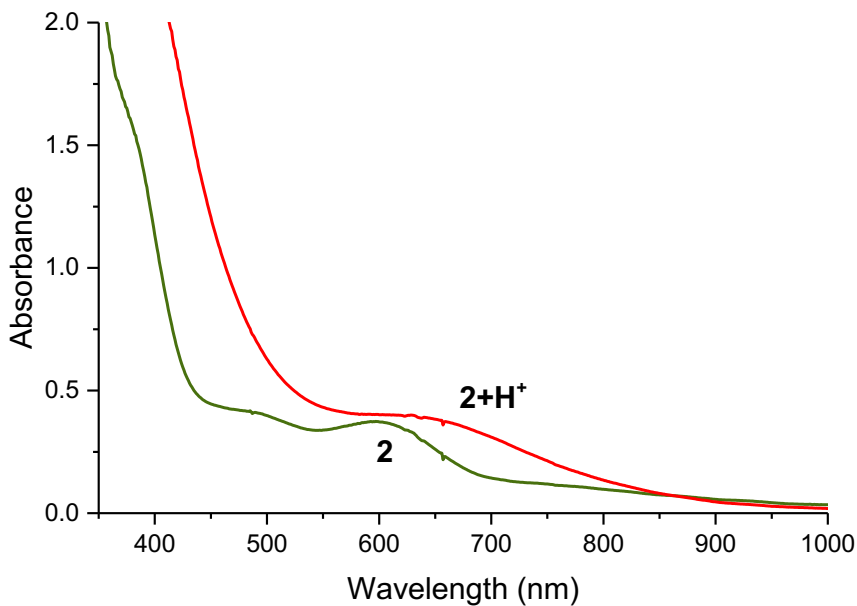


Figure S14: UV-vis spectra of the **2+H⁺** (red) observed upon addition of $\text{Sc}(\text{OTf})_3$ to **2** (green) in the presence of 0.2 M water at -40°C . **2** was generated by adding (1.5 eq) DBU/ H_2O to a 1 mM solution of **1** in CH_3CN .

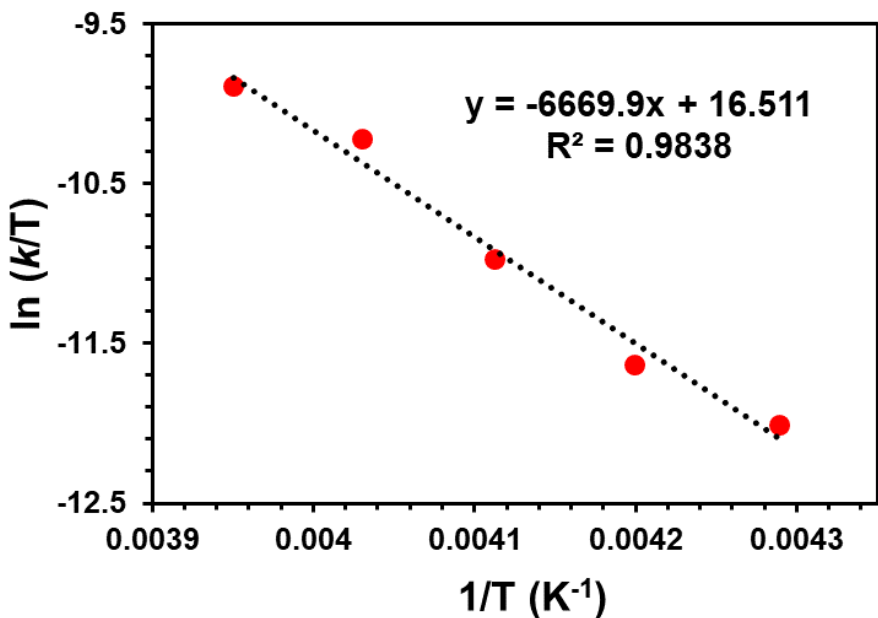


Figure S15: Eyring plot for the generation of **3** from **2** in CH₃CN from -40 °C to -20 °C by monitoring the 600-nm chromophore associated with **3**, the analysis of which affords $\Delta H^\ddagger = 55(2)$ kJ mol⁻¹ and $\Delta S^\ddagger = -62(10)$ J K⁻¹ mol⁻¹.

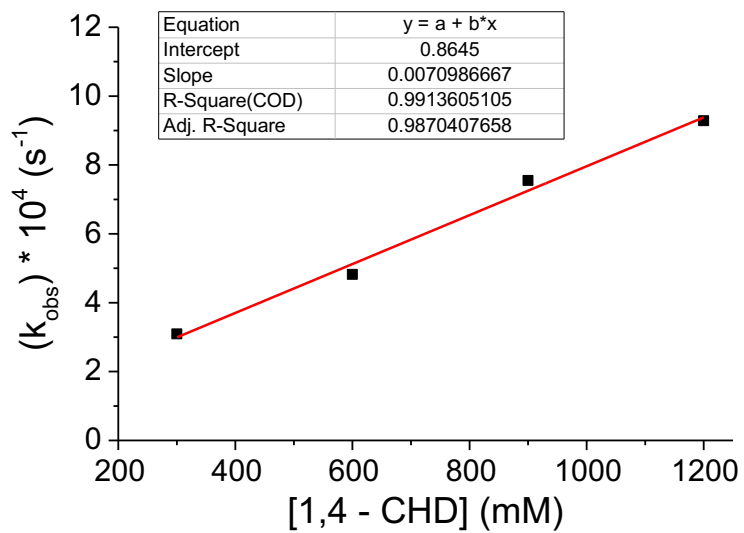


Figure S16: Second-order rate constants for the reaction of **3** with 1,4-cyclohexadiene in CH₃CN at -40°C.

5. DFT Calculations and Results

All coordinates and related data will be uploaded onto iochem-bd.org. All DFT calculations were performed with the Amsterdam Density Functional (ADF),^{1,2} and QUILD³s programs. Molecular orbitals were expanded in an uncontracted set of Slater type orbitals (STOs) of triple- ζ quality with double polarization functions (TZ2P).^{4,5} Core electrons were not treated explicitly during the geometry optimizations (frozen core approximation²). An auxiliary set of s, p, d, f, and g STOs was used to fit the molecular density and to represent the Coulomb and exchange potentials accurately for each SCF cycle.

Geometries of all possible spin states were optimized with the QUILD³ program using adapted delocalized coordinates until the maximum gradient component was less than 10^{-4} a.u. Energies, gradients and Hessians⁶ (for vibrational frequencies, including the Raman intensities) were calculated using S12g,⁷ in all cases by including solvation effects through the COSMO⁸ dielectric continuum model with appropriate parameters for the solvents.⁹ For computing Gibbs free energies, all small frequencies were raised to 100 cm⁻¹ in order to compensate for the breakdown of the harmonic oscillator model.^{10,11} Scalar relativistic corrections have been included self-consistently in all calculations by using the zeroth-order regular approximation (ZORA)¹². For all calculations carried out with S12g the Becke^{13,14} grid of VeryGood quality was used, except the calculations of the frequencies which were performed with a Becke grid of Normal quality.

All DFT calculations were performed using the unrestricted Kohn-Sham scheme. In case of the anti-ferromagnetically coupled systems, a locally adapted version of QUILD could be used that allows for geometry optimization using the SpinFlip approach¹⁵ within ADF: at each geometry iteration first a high-spin (all-up) calculation is done, whose orbitals and densities are then used to do a restart (at the same geometry!) where one of the Fe atoms has the spin densities change sign (from spin-up to spin-down) to lead to the open-shell singlet state; the geometry optimization and vibrational frequencies only involve the energy, gradients and Hessians of this second job at each (geometry iteration) step. However, a faster route to achieving the same results was used which involves the ModifyStartPotential where starting densities on the Fe atoms were prepared with spin-up density on one, and spin-down on the other.

All computational data have been uploaded (DOI: 10.19061/iochem-bd-4-15, link: <http://www.dx.doi.org/10.19061/iochem-bd-4-15>) onto the IOCHEM-BD platform (www.iochem-bd.org) to facilitate data exchange and dissemination, according to the FAIR principles¹⁶ of OpenData sharing.

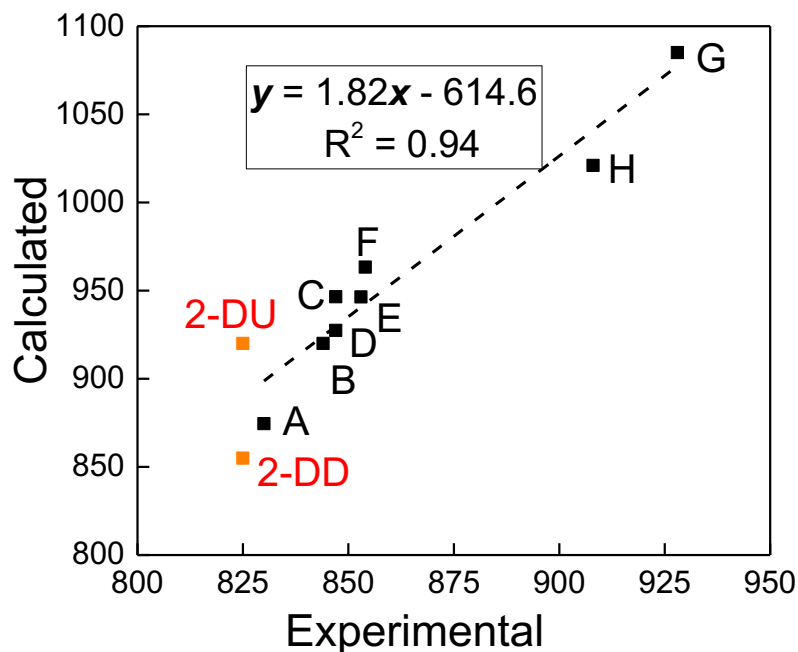


Figure S17: Correlation between experimental and theoretically calculated frequencies for O–O vibrations for the peroxodioiron(III) complexes (dashed line). Two different configurations of **2**, corresponding to the DU and DD conformations, are labelled in red. The other complexes have been labelled in black. The linear correlation suggests that the computation methods used here can account for the vibrational features amongst the complexes discussed in the discussion in the main text.

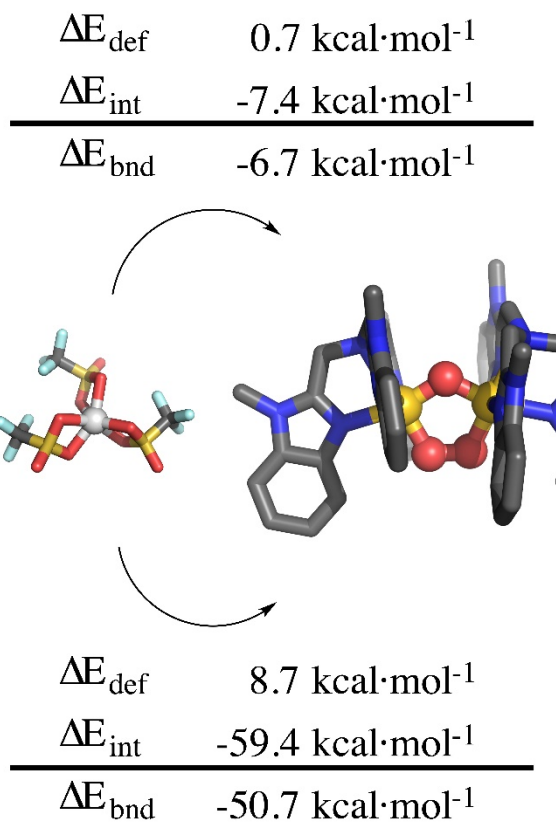


Figure S18: DFT structures of **2** indicating the preference of Sc^{3+} for binding to the peroxy ligand over the oxo ligand.

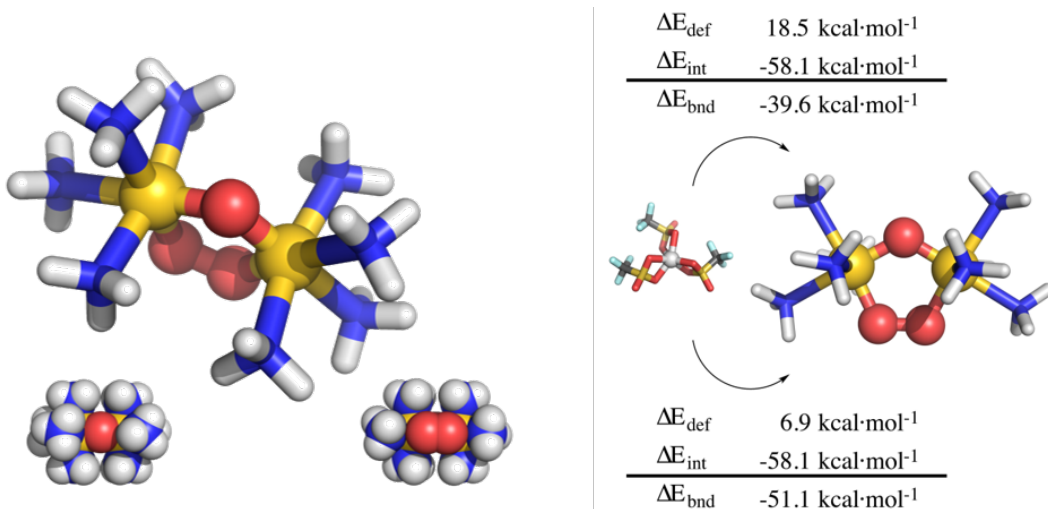


Figure S19: DFT structures of **m2**, showing the preference of Sc^{3+} for binding to the peroxy ligand over the oxo ligand

Table S4: Theoretically calculated frequencies for O–O vibrations and comparison with the experimentally obtained values.

Complex	Experimental	Calculated	Factor
2-DD	825	855	0.9649
2-DU	825	920	0.8967
A	830	874.5	0.9491
B	844	920	0.9174
C	847	946.5	0.8949
D	847	927.4	0.9133
E	853	946.4	0.9013
F	854	963.3	0.8865
G	928	1085	0.8553
H	908	1021	0.8893

Table S5: Comparison of vibrational frequencies from experiment and DFT for **3** and **m3**^a

Assignment ^b	m3 (DFT ^c)	3 (DFT ^b)	3 (exp.)
Antisymmetric stretch, v ₂	517 (-20)	531 [-24]	528 [-17]
v ₄	568 (-17)	556 [-23]	
v ₁	583 (-24)	663 [-24]	
Symmetric diamond core, v ₃	645 (-22) 673 (-10)	664 [-33]	653 [-30]

a) Indicated in square brackets are the ¹⁸O isotope shifts; b) Numbers given to v₁-v₅ correspond to the normal mode displacement vectors as shown in Figure 7 in the main text and Figure S20, with numbers consistent with ref ¹⁷ c) Obtained at S12g/TZ2P

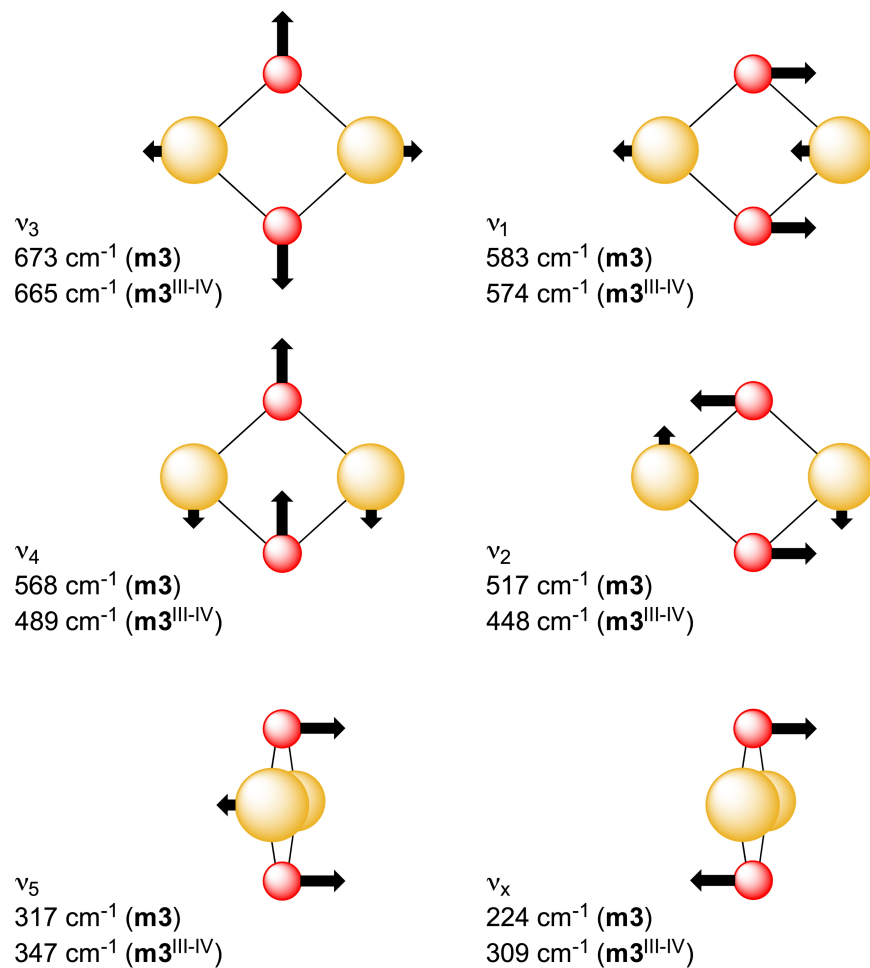


Figure S20. Atomic displacement vectors for the normal modes calculated for **m3** and **m3**^{III/IV}; the numbers in the labels follow those reported in ref¹⁷

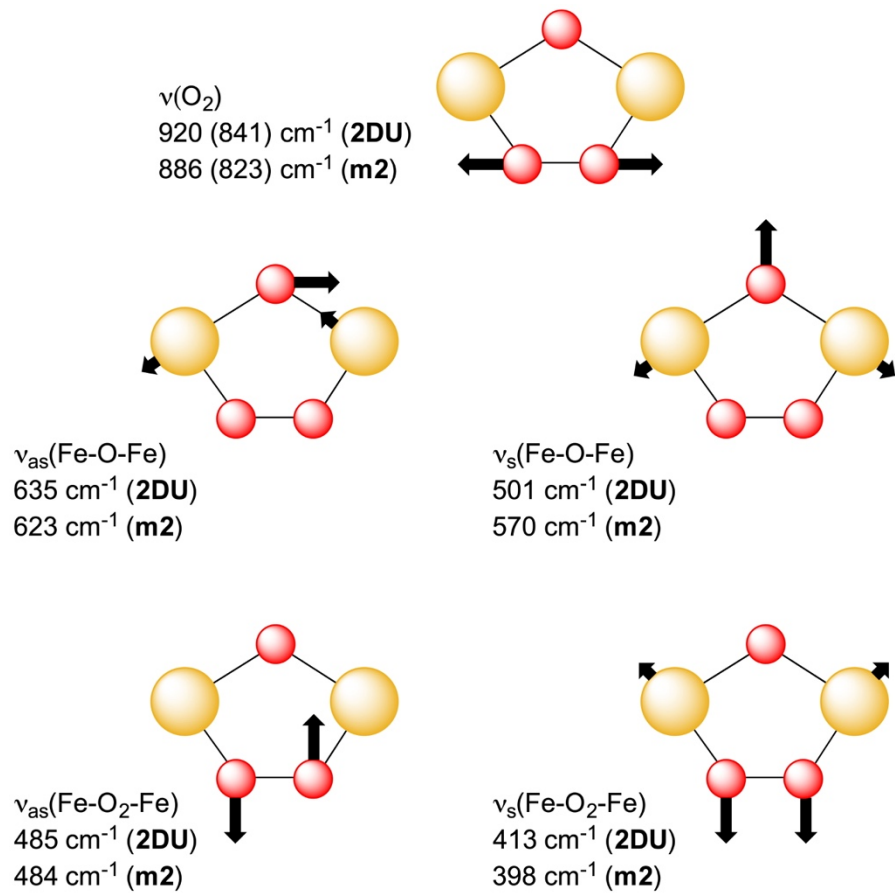


Figure S21. Atomic displacement vectors for the normal modes calculated for **2DU** and **m2** (similar modes were observed for the other μ -oxo diiron(III) complexes, see Table S6)

Table S6. Computed vibrational frequencies (cm^{-1}) at S12g/TZ2P with COSMO solvation included (acetonitrile)

complex	ν_{sym}	ν_{asym}	ν_{sym}	ν_{asym}	R (Å)	\angle (°)	R (Å)
	Fe-O ₂ -Fe	Fe-O ₂ -Fe	Fe-O-Fe	Fe-O-Fe	Fe-Fe	Fe-O-Fe	O-O
μ -oxo diiron(III) complexes							
2-DU	413.3	485.2	501.4	635.0	3.086	118.4	1.385
2-DD	436.8	509.2	523.2	634.1	3.100	121.3	1.395
m2	398.4	484.4	570.2	622.5	3.130	121.0	1.395
A BPPE	406.2	499.1	556.4	601.4	3.000	114.9	1.397
B BQPA	414.2	499.6	522.5	606.3	3.102	119.5	1.383
C 6Me3TPA	417.9	510.8	510.8	617.3	3.149	121.8	1.370
D 6Me2BPP	403.0	492.1	496.4	618.7	3.163	121.9	1.381
E 6MeBQPA	421.4	499.4	509.7	619.4	3.132	121.0	1.372
F BnBQA	406.1	495.9	517.7	621.9	3.135	121.6	1.368
μ -hydroxo diiron(III) complexes							
2+H⁺	493.9	395.7	319.2	471.5	3.255	106.2	1.370
m2+H⁺	419.1	467.2	374.9	407.1	3.505	121.1	1.339
G BnBQA	431.0	470.4	431.0	404.9	3.529	122.5	1.323
H 6Me2BPP	384.8	473.4	445.2	473.4	3.534	121.3	1.346

Table S7. Computed Mössbauer parameters ($\text{mm}\cdot\text{s}^{-1}$) at S12g/TZ2P with COSMO solvation included (acetonitrile)

complex	Isomer shift (δ)	Quadr. Spl. (ΔE_Q)
μ -oxo diiron(III) complexes		
2-DU	0.466, 0.448	0.800, 0.953
2-DD	0.437, 0.437	1.384, 1.382
m2	0.502, 0.502	1.161, 1.172
A BPPE	0.497, 0.504	1.282, 1.297
B BQPA	0.451, 0.427	1.659, 1.466
C 6Me3TPA	0.475, 0.445	1.495, 1.359
D 6Me2BPP	0.496, 0.501	1.308, 1.440
E 6MeBQPA	0.478, 0.442	1.481, 1.206
F BnBQA	0.485, 0.488	1.167, 0.919

μ -hydroxo diiron(III) complexes		
2+H⁺	0.476, 0.510	1.173, 1.146
m2+H⁺	0.540, 0.539	1.029, 1.035
G BnBQA	0.553, 0.533	1.407, 0.695
H 6Me2BPP	0.573, 0.506	1.447, 1.151
diamond core diiron(IV) complexes		
3-DU^a	-0.046, -0.046	2.119, 2.116
3-DD^b	0.010, 0.010	1.813, 1.808
m3	0.050, 0.049	1.963, 1.969

a) Relative energy 0.0 kcal·mol⁻¹; b) Relative energy +16.1 kcal·mol⁻¹

6. References

- (1) Baerends, E. J.; Ziegler, T.; Autschbach, J.; Bashford, D; Bérçes, A.; Bickelhaupt, F. M.; Bo, C.; Boerrigter, P. M.; Cavallo, L.; Chong, D. P.; Deng, L.; Dickson, R. M.; Ellis, D. E.; van Faassen, M.; Fan, L.; Fischer, T. H.; Fonseca Guerra, C.; Ghysels, A.; Giammona, A.; van Gisbergen, S. J. A.; Götz, A. W.; Groeneveld, J. A.; Gritsenko, O. V.; Grüning, M.; Gusarov, S.; Harris, F. E.; van den Hoek, P.; Jacob, C. R.; Jacobsen, H.; Jensen, L.; Kaminski, J. W.; van Kessel, G.; Kootstra, F.; Kovalenko, A.; Krykunov, M. V.; van Lenthe, E.; McCormack, D. A.; Michalak, A.; Mitoraj, M.; Neugebauer, J.; Nicu, V. P.; Noddeman, L.; Osinga, V. P.; Patchkovskii, S.; Philipsen, P. H. T.; Post, D.; Pye, C.C.; Ravenek, W.; Rodríguez, J.I.; Ros, P.; Schipper, P.R.T.; Schreckenbach, G.; Seldenthuis, J.S.; Seth, M.; Snijders, J. G.; Solà, M.; Swart, M.; Swerhone, D.; te Velde, G.; Vernooijs, P.; Versluis, L.; Visscher, L.; Visser, O.; Wang, F.; Wesolowski, T.A.; van Wezenbeek, E.M.; Wiesenecker, G.; Wolff, S. K.; Woo, T.K.; Yakovlev A.L. ADF2012, SCM, Theoretical Chemistry, Vrije Universiteit, Amsterdam, The Netherlands, <http://www.scm.com>
- (2) te Velde, G.; Bickelhaupt, F. M.; Baerends, E. J.; Fonseca Guerra, C.; van Gisbergen, S. J. A.; Snijders, J. G.; Ziegler, T. Chemistry with ADF. *J. Comput. Chem.* **2001**, 22 (9), 931–967.
- (3) Swart, M.; Bickelhaupt, F. M. QUILD: Quantum-Regions Interconnected by Local Descriptions. *J. Comput. Chem.* **2008**, 29 (5), 724–734.
- (4) Van Lenthe, E.; Baerends, E. J. Optimized Slater-Type Basis Sets for the Elements 1–118. *J. Comput. Chem.* **2003**, 24 (9), 1142–1156.
- (5) Chong, D. P.; Van Lenthe, E.; Van Gisbergen, S.; Baerends, E. J. Even-Tempered Slater-Type Orbitals Revisited: From Hydrogen to Krypton. *J. Comput. Chem.* **2004**, 25 (8), 1030–1036.
- (6) Wolff, S. K. Analytical Second Derivatives in the Amsterdam Density Functional Package. *Int. J. Quantum Chem.* **2005**, 104 (5), 645–659.
- (7) Swart, M. A New Family of Hybrid Density Functionals. *Chem. Phys. Lett.* **2013**, 580, 166–171.
- (8) Klamt, A.; Schüürmann, G. COSMO: A New Approach to Dielectric Screening in Solvents with Explicit Expressions for the Screening Energy and Its Gradient. *J. Chem. Soc. Perkin Trans. 2* **1993**, No. 5, 799–805.
- (9) Swart, M.; Rösler, E.; Bickelhaupt, F. M. Proton Affinities in Water of Main-group-Element Hydrides - Effects of Hydration and Methyl Substitution. *Eur. J. Inorg. Chem.* **2007**, No. 23, 3646–3654.
- (10) Averkiev, B. B.; Truhlar, D. G. Free Energy of Reaction by Density Functional Theory: Oxidative Addition of Ammonia by an Iridium Complex with PCP Pincer Ligands. *Catal. Sci. Technol.* **2011**, 1 (8), 1526–1529.
- (11) Klein, J. E. M. N.; Dereli, B.; Que, L.; Cramer, C. J. Why Metal-Oxos React with Dihydroanthracene and Cyclohexadiene at Comparable Rates, despite Having Different C-H Bond Strengths. A Computational Study. *Chem. Comm.* **2016**, 52 (69), 10509–10512.
- (12) Lenthe, E. Van; Baerends, E. J.; Snijders, J. G.; Lenthe, E. Van; Baerends, E. J.;

- Snijders, J. G. Relativistic Regular Two-Component Hamiltonians. *J. Chem. Phys.* **1993**, *99*, 4597–4610.
- (13) Franchini, M.; Philipsen, P. H. T.; Visscher, L., The Becke Fuzzy Cells Integration Scheme in the Amsterdam Density Functional Program Suite. *J. Comput. Chem.* **2013**, *34* (21), 1819–1827.
- (14) Becke, A. D. A Multicenter Numerical Integration Scheme for Polyatomic Molecules. *J. Chem. Phys.* **1988**, *88* (4), 2547–2553.
- (15) Hopmann, K. H.; Pelmenschikov, V.; Du, W.-G. H.; Noddleman, L. in Spin States in Biochemistry and Inorganic Chemistry: Influence on Structure and Reactivity, Eds. M. Swart and M. Costas; John Wiley & Sons: Chichester, UK, 2016; pp 297–325.
- (16) Wilkinson, M. D.; Dumontier, M.; Aalbersberg, I. J.; Appleton, G.; Axton, M.; Baak, A.; Blomberg, N.; Boiten, J.-W.; da Silva Santos, L. B.; Bourne, P. E.; Bouwman, J.; Brookes, A. J.; Clark, T.; Crosas, M.; Dillo, I.; Dumon, O.; Edmunds, S.; Evelo, C. T.; Finkers, R.; Gonzales-Beltran, A.; Gray, A. J. G.; Groth, P.; Goble, C.; Grethe, J. S.; Heringa, J.; 't Hoen P. A.; Hooft, R.; Kuhn, T.; Kok, R.; Kok, J.; Lusher, S. J.; Martone, M. E.; Mons, A.; Packer, A. L.; Persson, B.; Rocca-Serra, P.; Roos, M.; van Schaik, R.; Sansone, S.-A.; Schultes, E.; Sengstag, T.; Slater, T.; Strawn, G.; Swertz, M. A.; Thompson, M.; van der Lei, J.; van Mulligen, E.; Velterop, J.; Waagmeester, A.; Wittenburg, P.; Wolstencroft, K.; Zhao, J.; Mons, B. The FAIR Guiding Principles for Scientific Data Management and Stewardship. *Sci. Data* **2016**, *3* (1), 160018.
- (17) Wilkinson, E. C. Raman Signature of the Fe_2O_2 “diamond” Core. *J. Am. Chem. Soc.* **1998**, *120* (5), 955–962.